Discharge Flow Measurements of a Centrifugal Turbomachinery

Jong-Soo Choi*

(*Received July 23, 1993*)

The objective of this research is to obtain a better insight into the structure of the flowfield in a centrifugal turbomachinery. To investigate this turbomachinery flowfield, measurements have been made with hot-wire sensors at the exit of a centrifugal impeller. The measured data at the discharge show a jet-wake type of flow pattern which results in a strong vorticity field. The flow with high velocity found on the pressure side tends to move to the low pressure region present at the suction side of an impeller blade as a form of roll-up around the blade trailing edge. This flow motion is believed to cause an unsteady flow separation at the suction side of the blade and consequently to disturb the flow in the adjacent passage.

Key Words: Centrifugal Impeller, Centrifugal Turbomachinery, Discharge Flow, Secondary Flow, Jet and Wake Flow

Nomenclature

b : Impeller blade width
D : Impeller diameter
p : Static pressure
Q : Volume flow rate
r : Radius in cylindrical coordinates
R : Impeller radius
U : Velocity in rotating coordinates
V : Velocity in stationary coordinates
z : Axial distance from the shroud
Δr : Radial distance from the impeller tip
ϕ : Flow coefficient ($Q/\pi bDV_{tip}$)
ψ : Pressure rise coefficient ($\Delta p/\rho V_{tip}^2$)
ω_z : Vorticity strength in z-direction
Ω : Angular rotational speed of the impeller
ρ : Fluid density

Subscripts

r : Radial
t : Tangential
tip : Property at the tip of impeller

Superscripts

$\sim$: Periodically fluctuating component
$-$: Steady state average
$''$: Instantaneous value

* The Pennsylvania State University, Currently in Chungnam National University

1. Introduction

Centrifugal turbomachines are widely used due to their ability to generate relatively high pressure ratios in a short axial distance compared to axial compressors. They are often found in gas turbine engines, heating ventilation and air conditioning systems, and pumps. In order to improve the performance of centrifugal turbomachinery, extensive theoretical and experimental work has been conducted to characterize the discharge flow.

Many researchers have found that the discharge from a centrifugal impeller is composed of a high speed jet region and a low speed wake. The formation of the wake region in a passage was explained by Fowler(1968) as being due to the flow on the high pressure side rolling over the tip of the impeller blade and flowing back into the low-pressure zone of the adjacent passage. It has also been postulated that the secondary flow in the impeller blade passage carries hub and shroud boundary layers to the suction side of the impeller blade to form a low velocity region (McDonald, Lennemann and Howard, 1971; Johnson and Moore, 1983a). Secondary flow in centrifugal

impellers develops due to the rotation of the impeller and the physical curvature of the impeller geometry (Johnson and Moore, 1983b).

In addition to the aforementioned theoretical and experimental efforts, several computational attempts have been developed recently to simulate the flowfield in centrifugal impellers and diffusers (Jorgenson and Chima, 1989; Hah and Krain, 1989). The capability of these schemes is still far from satisfactory to accurately predict the flowfield, however. The complicated three-dimensional flow in the blade passages and the potential for strong interaction between adjacent passages at the discharge are the main problems that cause the efforts to be unsuccessful.

The overall performance of a centrifugal turbomachine not only depends on the impeller flow but also depends on the efficiency of a diffuser. The purpose of a diffuser is to recover the kinetic energy of the discharged flow from the impeller and convert it to static pressure. A diffuser may be fitted with vanes depending on the size, speed and pressure ratio of the system (Japikse, 1984). The spatially non-uniform flow discharged from the impeller can induce unsteady flow fluctuations in the diffuser that can significantly alter the nature of the flow. The nature of the flow unsteadiness is not well known but the flow entering the diffuser has been postulated to interact with the boundary layer on the diffuser walls, and often induce flow separation. The centrifugal impeller discharge flow in both vaned and vaneless diffusers has been investigated in detail by Inoue and Cumpsty(1984).

As discussed above, the presence of a vaneless or vaned diffuser influences the flowfield inside of the impeller passages, which makes it difficult to understand the nature of the flow. Since the objective of this research was to characterize the flowfield discharged from a centrifugal impeller, the impeller was tested without a diffuser or casing. In addition to developing some fundamental understanding, the study has direct application to the class of centrifugal turbomachines that collect the discharged fluid without a cut-off on the volute and without diffuser stator vanes. The effect of discharge configurations on the flowfield can be realized based on the present results, and is being examined in a continuing study by Bent(1993).

2. Experimental Facility and Procedure

2.1 Test facility

For the experiments, a commercial water pump impeller (Worthington Model D-1011) was chosen (Fig. 1). The impeller has seven backward swept blades with a discharge angle of about 21 degrees to the tangent. The impeller has a curved front shroud while the hub is relatively flat and perpendicular to the inlet flow direction. The inlet and discharge diameters of the impeller are 133.4 mm and 320.0 mm, respectively.

An experimental facility is designed to power a centrifugal impeller without an outer casing at any rotational speed up to 3600 rpm. The rotational speed of the impeller is measured with an optical shaft encoder placed between the motor and the bearings. The shaft encoder emits a five volt pulse every revolution. This is sampled simultaneously with the other signals from the sensors and is used to measure the shaft speed.

The inlet flow is controlled by an upstream flow management unit, including a bellmouth inlet, turbulence management screens, honeycomb and a duct. The volumetric flow rate Q is obtained from the static pressure difference and

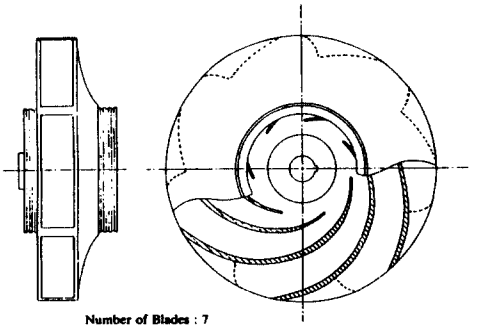

	Diameter	Blade Angle	Blade Width
Inlet	133.4 mm	11 deg.	57 mm
Discharge	320.0 mm	21 deg.	40 mm

Fig. 1 Tested centrifugal impeller

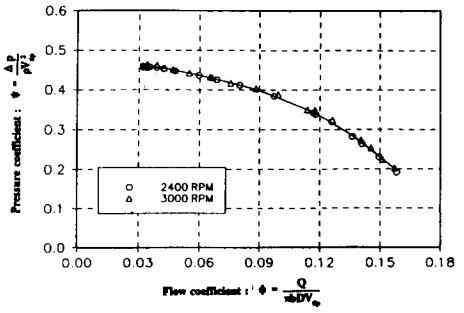

Fig. 2 Performance characteristics of the impeller

the cross sectional area ratio measured at the neckdown. The impeller performance characteristics are determined by the static pressure difference (Δp) between the impeller inlet and the discharge at various flow rates. The non-dimensional static pressure rise through the impeller ($\psi = Q/\pi bDV_{tip}$), plotted versus flow coefficient ($\phi = p/\rho V_{tip}^2$) constitutes the non-dimensional operating curve for the impeller. The curves at two different shaft speeds collapse well, which suggests that the non-dimensional parameters have been properly chosen (Fig. 2). From manufacturer's data it was determined that the impeller was originally designed to have maximum efficiency at $\phi = 0.062$.

A digital data acquisition and analysis system based on an IBM PC/AT compatible computer and a Metrabyte DAS-20 12 bit A/D converter is used to acquire and analyze data. To avoid aliasing problems in digital signal processing, low pass analog filters (Ithaco Model 4302) are used in all measurements.

2.2 Instrumentation

Hot-wire sensors are ideal for the measurement of turbomachinery flows because of their high frequency response, low noise level, and fine spatial resolution. There are many different types of hot-wire sensor configurations from which to choose. In the experiment described below, the unsteady discharge flowfield was measured with a crossed hot-wire probe (TSI Model 1241-T1.5). This crossed-wire probe is designed to simultaneously measure two components of the instantaneous flow velocity. The crossed-wire probe calibration procedure and data processing techniques used in these experiments followed those of Westphal and Mehta(1984). Once the probe has been calibrated, a check is made on its accuracy by varying the probe angle in the calibration jet and comparing the estimated velocity with the true velocity. The measuring accuracy of the velocity magnitude and yaw angle are $\pm 2\%$ and ± 2 deg., respectively, for yaw angles up to ± 35 degrees.

The radial and tangential velocity components and turbulence quantities at the impeller discharge are obtained from the velocity magnitude and relative angle measured with the crossed-wire probe. In order for the flow to be within the crossed-wire probe sensitive range, the probe angle was set to 20 degrees from the tangent of the impeller circumference. In this way data are reliable for flow discharge angles from -15 to 55 degrees for the error range mentioned above.

2.3 Phase averaging and coordinate transformation

The hot-wire data measured at the impeller discharge have strong periodicity at the impeller blade rate. This was determined from the measured signal by using a synchronous averaging technique. This technique isolates a periodic signal at the synchronized frequency and its harmonics from the measured signal that contains many other frequencies. All hot-wire data were sampled in conjunction with a signal from a shaft encoder which generated a 5 volt pulse once per revolution of the impeller. This signal is used as a reference to average the hot-wire data for a certain number of revolutions.

The phase averaging technique has been widely used for analyzing the inlet and discharge flow in both axial and centrifugal turbomachinery flowfields. This technique decomposes a measured instantaneous flow velocity (u) into a circumferential mean ($\bar{U}$), an averaged spatial variation ($\tilde{U}$), and a perturbation on top of these mean values (u'),

$$u(\theta, t) = \bar{U} + \tilde{U}(\theta) + u'(\theta, t)$$

The $\bar{U}$ is periodic at the synchronizing frequency (shaft rate) and has zero mean value. The perturbation term u' therefore represents any flow

unsteadiness not synchronized with the shaft rate. In contrast to the time dependent u', the remaining two ensemble averaged values can be represented with a single time independent parameter U,

$$U(\theta)=\bar{U}+\tilde{U}(\theta)$$

This mean value U is a function of azimuthal location and will be used hereafter to represent the phase averaged mean velocity at the discharge. The averaging technique significantly reduces the random fluctuations superposed on the periodic signal. Since more than 100 averages showed little effect on the averaged data, the mean velocity data presented in this paper are averaged over 100 impeller revolutions. The velocitydistribution information is more easily understood by converting the measured data from the laboratory coordinate frame to a frame of reference on the impeller. In this transformation, the radial component of the velocity is identical in both the stationary and rotating coordinate frames. The tangential component in relative coordinates is found from the following relationship,

$$U_t=(R+\Delta r)\Omega-V_t\equiv r\Omega-V_t$$

where Ω is the angular rotational speed of the impeller, R is the impeller radius, Δr is the radial distance from the impeller trailing edge, so $r=R+\Delta r$.

3. Experimental Results and Discussion

3.1 Character of flow in an impeller passage

Figure 3 shows the measured synchronous averaged discharge velocity magnitude in the stationary (laboratory) coordinate frame at various radial positions. These data transformed into the rotating (impeller) coordinate frame are shown in Fig. 4. The probe was placed at the mid-passage, i.e., $z/b=0.5$, and the impeller was operated at the flow rate $\phi=0.06$. The same experiment was repeated for higher flow rates $\phi=0.09$ and $\phi=0.12$ and showed a highly repetitive flow pattern from blade passage to blade passage.

The impeller tip speed was used to non-

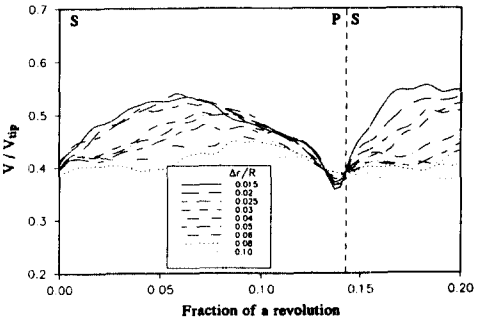

Fig. 3 Measured discharge velocity amplitudes in stationary coordinates

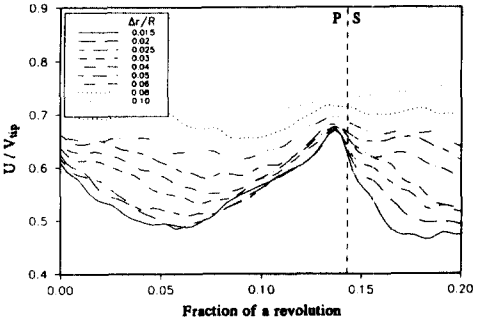

Fig. 4 Measured discharge velocity amplitudes in rotating coordinates

dimensionalize these quantities. The horizontal scale, marked fraction of a revolution, begins at the trailing edge of impeller blade #1. The location of the second blade trailing edge, is marked with a vertical dotted line. This is a result of synchronizing the shaft encoder signal with the # 1 blade when the blade is aligned with the hot-wire probe. The horizontal scale therefore can be replaced with angular position, θ, which is measured from a radial line passing the trailing edge of the #1 blade. The data on the figure is the quantity measured when the corresponding point on the impeller ($\theta/360$ or fraction of a revolution) passes by the hot-wire probe. The pressure and suction sides of each blade are marked with P and S on opposite sides of the dotted lines, respectively. The pressure side corresponds to the convex side of a blade, because the blades are swept backward.

The discharge velocity pattern (in rotating

coordinates), shown in Fig. 4, clearly shows a high velocity (jet) region near the pressure side of a blade compared to the low velocity (wake) region in the suction side. At all three flow rates, the discharge flowfield shows a shear region on either side of the jet. Especially, a high shear region is found near the trailing edge of each blade where mixing between the jet and wake occurs. This flow mixing is so rapid that the jet-wake pattern cannot be identified even before the flow reaches a distance of 10% of the radius from the impeller. The measurements taken at the closest location to the impeller, $\Delta r/R=0.015$, show the jet-wake flow structure clearly for all three cases. The region near the suction side of the trailing edge, however, does not show a defined blade wake emanating from the trailing edge. Similar observations have been made by Maksoud and Johnson(1987). Their three-component hot-wire measurements show a secondary flow pattern which results in a flow from hub to shroud on the suction side and in the opposite direction on the pressure side. This secondary motion is generated by the centrifugal and Coriolis effects. The shearing action between the opposed secondary flows contributes to the fast wake mixing in the discharge.

The jet-wake flow pattern can be more clearly identified with the velocity contours shown in Fig. 5. Three flow rate cases are compared for the measurements taken with the crossed-wire probe over roughly two impeller passages. For each figure the velocity data in rotating coordinates measured at seven equally spaced axial locations from hub to shroud are used. The contour levels below the spatial mean velocity are shaded in the figure to show the low velocity region. At low flow rate $\phi=0.06$, the discharge flow is more evenly distributed over the entire passage compared with the other higher flow rate cases. The wake region is located in the middle of the passage while the high velocity region is confined near the hub/pressure-side corner. In contrast, when the flow rate is increased to $\phi=0.12$, a distinct wake region is developed near the shroud adjacent to the suction surface of the blade, and the jet region dominates half of the pressure side of the passage.

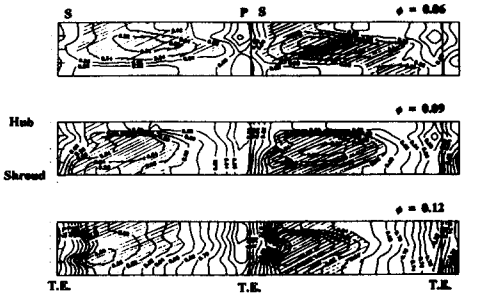

Fig. 5 Relative velocity contour ($\Delta r/R=0.02$)

This jet and wake type of flow pattern has been observed by many other investigators in centrifugal turbomachinery experiments. Fowler(1968) tested a radial channel with and without the influence of adjacent channels and found that the suction side flow detachment is affected largely by the flow from the adjacent channels. McDonald, Lennemann and Howard(1971) also found the wake region at mid-blade height on thesuction surface. The formation of wake region was explained by the effect of the secondary flow which carried hub and shroud boundary layers to the suction surface. The location of the wake is, however, known to be influenced by the flow rate and the running speed as well as the impeller geometry. Johnson and Moore(1983a) found that the wake region located in the middle of the passage near the suction surface at a low flow rate was moved toward the suction-surface/shroud corner as the flow rate is increased. This is the same trend that is observed in the present experiment. They concluded that the relative magnitude of the secondary flow due to rotation and impeller curvature generated in the axial to radial bend are responsible for the wake's position.

Figure 6 depicts the velocity direction β calculated from the velocity component measurements when $\beta=0$ corresponds to the direction tangent to the impeller circumference. When the jet side flow passes near the trailing edge of a blade, the angle becomes smaller due to the lower pressure on the suction side of the blade. This is shown with the phase-averaged discharge angle of the flow in Fig. 6. For comparison, the flow angles in rotating coordinate are shown at three radial

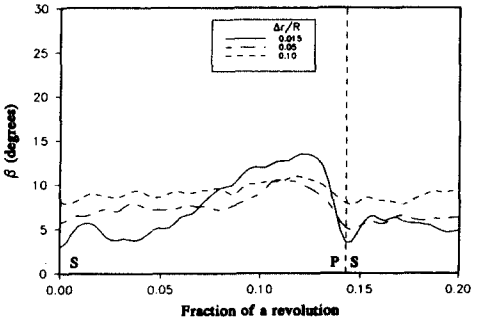

Fig. 6 Measured discharge flow angles in rotating coordinates

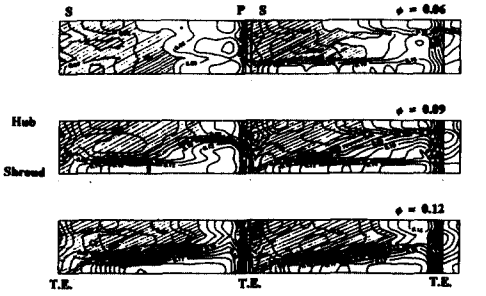

Fig. 7 Radial velocity contour ($\Delta r/R=0.02$)

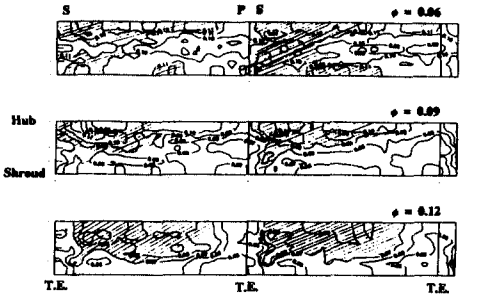

Fig. 8 Turbulence intensity contour ($\Delta r/R=0.02$)

locations for a flow rate of $\phi=0.06$. The discharge angle in rotating coordinates is much less than the blade angle, which is 21 degrees to the tangent. This is presumably due to the discharge configuration not having a diffuser which promotes fast flow diffusion. The angle shows substantial variation along the impeller circumference when it is measured close to the impeller. This spatial distribution of the angle quickly becomes uniform as the flow moves downstream. A high discharge angle (between 10 to 15 degrees) is found in the jet region, while the angle near the wake is very small (about 5 degrees). The region immediately behind the trailing edge has the smallest flow angle. Further discussion of this high shear region will be presented later in this paper.

From the measured velocity magnitude and angle, the radial and tangential component of the discharge velocities can be obtained. The radial velocity is found to be much smaller than the tangential velocity. At $\phi=0.06$, as an example, the spatially averaged radial velocity is about 7% of the impeller tip speed compared to 50% for the tangential velocity in rotating coordinates. Figure 7 shows the radial velocity contours distributed over approximately two passages from shroud to hub. Once again the region where the radial velocity is lower than the spatial average is shaded. The low radial velocity region is distributed over the half of the passage area close to the suction side at $\phi=0.06$. This moves to the hub/suction-side corner as the flow rate increases. This trend is comparable to the effect of the flow rate on the location of the high turbulence intensity region shown in Fig. 8. For each flow rate, the high turbulence region (shaded area) is located where the radial velocity is found to be low. This implies that the high radial velocity region of the flow tends to be more stable than the flow in the low radial velocity region. This may be due to the influence of the adjacent passages, which is morelikely where the radial velocity is low. The proposed flow behavior is observed from the time trace of the instantaneous radial velocity. A negative radial velocity is found intermittently near the suction side and is apparent in all three flow rate cases. This unsteady backflow is believed to disturb the passage flow, and consequently induce unsteady pressure fluctuations on the blade surface. The unsteady flow behavior and the effect on the generated noise are examined and reported in Choi(1991).

It is also found that the overall turbulence intensity level is higher at low flow rates. The low flow momentum through the blade passage, which would promote thick boundary layers on

the passage walls, may be responsible for this flow behavior. The boundary layers are then mixed out by the secondary flow before they reach the discharge.

The presence of the secondary flow in the impeller passage can be implied from the tangential velocity profiles in rotating coordinates. Figure 9 shows the deviation of tangential velocities from the spatial mean over the entire discharge area. In the figure, nine equally spaced circumferential locations for each blade pitch are marked with vertical dashed lines. For each circumferential location, data are measured at nine axial locations from hub to shroud. The phase-averaged tangential velocity data measured at each location are then subtracted by the spatial mean tangential velocities. Therefore, the data on the left of the corresponding vertical line indicate the tangential velocity which is smaller than the spatial mean and vice versa. At $\phi=0.06$, a pair of counter-rotating vortices appear to be present. Specifically, the relative flow moves away from the pressure to the suction side in the middle of the blade height and returns to the pressure side along both the hub and shroud walls. This secondary flow pattern is less identifiable as the flow rate increases. The pattern is found in about half the suction side passage at $\phi=0.09$. The area becomes only one third of the passage at $\phi=0.12$. This is mainly due to the flow motion from the jet to the wake region caused by axial vorticity in the shear layer, which is added to the secondary flow

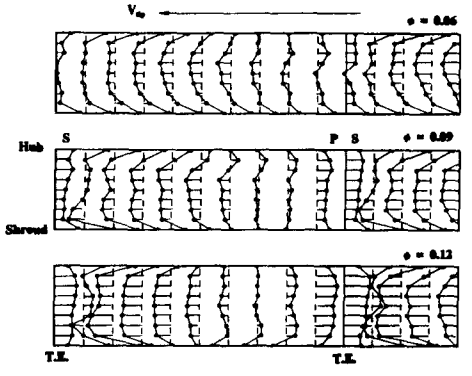

Fig. 9 Tangential velocity variation from spatial mean ($\Delta r/R=0.02$)

motion, the effect of which can be noticed at $\phi=0.12$ most easily where the jet-wake pattern is the strongest among the three flow rate cases. The flow near the pressure side of the blade has a larger tangential velocity than the spatial mean for all axial locations from hub to shroud. There is also a strong relative flow motion toward the wake region located at the shroud/suction-side corner. As a result, the secondary flow motion is less obvious in the discharge because of the effect of the axial vorticity near the trailing edge of the blade.

3.2 Axial vorticity distribution in the discharge

As shown in the previous section, the discharge flowfield shows a strong shear region on either side of the jet. This flowfield can be separated into a spatially uniform flow and a vortical flow motion. The average vorticity strength can be quantified by using the phase-averaged velocity components in relative coordinates. In mathematical form, two-dimensional vorticity whose axis is parallel to the trailing edge of blades (ω_z) can be defined as,

$$\omega_z \equiv \nabla \times \bar{U} = \frac{U_t}{r} + \frac{\Delta U_t}{\Delta r} = \frac{1}{r}\frac{\Delta U_r}{\Delta \theta}$$

Fig. 10 shows contours of axial vorticity at the mid-passage ($z/b=0.5$) of the impeller discharge for three flow rates. Each figure is generated from the radial and tangential components of velocities measured at 10 radial locations between $\Delta r/R=0.015$ and $\Delta r/R=0.1$. The scale of the y-axis in the figure is expanded by 5 times to clarify the vorticity distribution. For all three flow rates, the discharge flowfield is dominated by the positive axial vorticity, which is rotating in the clockwise direction in the figures. The negative vorticity region is not clearly observed on the figures, but is found in the small area at the middle of the blade to blade passage very near the impeller. As was expected from the velocity profiles in Fig. 4, a strong vorticity region is found near the trailing edge of the blades. At a high flow rate $\phi=0.12$, a region of strong vorticity is found near the suction side of the blade passage. This high vorticity region becomes evenly distributed around the impeller discharge as the flow rate is reduced. It is

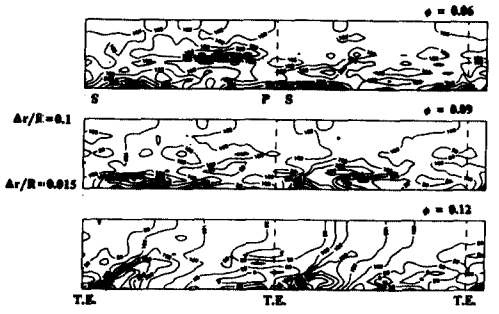

Fig. 10 Axial vorticity distribution at the discharge

also interesting to observe how quickly the vorticity strength is reduced as flow moves away from the impeller. Care must be taken, however, in interpreting the discharge vorticity field based on phase-averaged velocity data. This is because the phase averaging process removes the effect of all unsteady flow motion other than that at the synchronized frequency. More specifically, the vortices shed from the impeller cannot be captured by using the phase averaging technique unless they are synchronized with the impeller, while the vortices fixed at the same relative location to the rotating impeller can be. Shown in Fig. 10 are, therefore, the vortices that are bound in their relative locations, and their strengths are averaged over a period of time.

The instantaneous vorticity field in a vaneless diffuser of a centrifugal pump was measured by Paone et al.(1989). By using particle image displacement velocimetry (PIDV), they were able to measure instantaneous velocity vectors in a two dimensional plane. From this, the instantaneous vorticity was calculated. At a high flow rate, the results clearly showed propagation of axial vortices from the wakes of impeller blades. In the diffuser, the vorticity decayed progressively and spread out due to the mixing between the free stream and the wake. When the flow rate was reduced, vorticity was present throughout the field, from the impeller discharge to the diffuser exit. A similar trend is also found in the phase-averaged vorticity field shown in Fig. 10. The high vorticity region is limited to the suction side of a blade trailing edge at $\phi=0.12$, while the region is distributed over more than half of the impeller discharge at $\phi=0.06$.

4. Conclusions

The measured velocity data at the impeller discharge show a jet-wake flow pattern in a passage. At the low flow rate, $\phi=0.06$, the wake region is found in the middle of the passage while the high velocity region is confined near the hub/pressure side corner. When the flow rate is doubled to $\phi=0.12$, the wake moves toward the shroud adjacent to the suction surface of the blade and the jet region dominates a half of the pressure side of the passage. Measurements taken further from the impeller showed that this jet-wake flow pattern disappears quickly as the flow moves downstream. The secondary flow in the impeller passage is thought to be responsible for the rapid flow mixing. A region of strong axial vorticity was also found near the suction side of the impeller blade where a high velocity shear is present between the jet and wake flow. The vorticity was found to influence the flow discharging from the adjacent passage. The relatively small radial velocity and high level of turbulence intensity found in the flow on the suction side of a blade suggested a possible flow separation in this region. As a consequence of the shedding vorticity or the unsteady flow separation or both, the jet-wake flow in a passage may become unstable.

References

Bent, P. H., 1993, *The influence of the Discharge Configuration on the Generation of Broadband Noise in Centrifugal Turbomachinery*, Ph. D. Thesis, The Pennsylvania State University.

Choi, J. S., 1991, *Experiments on the Unsteady Flowfield Associated with Noise Generation in Centrifugal Turbomachinery*, Ph. D. Thesis, The Pennsylvania State University.

Fowler, H. S., 1968, "The Distribution and Stability of Flow in a Rotating Channel," ASME Journal of Engineering for Gas Turbine and Power, Vol. 90, No. 3, pp. 229~236.

Hah, C. and Krain, H., 1989, "Secondary

Flows and Vortex Motion in a High-Efficiency Backswept Impeller at Design and Off-Design Conditions," ASME Paper No. 89-GT-181.

Inoue, M. and Cumpsty, N. A., 1984, "Experimental Study of Centrifugal Impeller Discharge Flow in Vaneless and Vaned Diffusers," ASME Journal of Engineering for Gas Turbine and Power, Vol. 106, pp. 455~467.

Japikse, D., 1984, *Turbomachinery Diffuser Design Technology*, Concepts ETI Inc., Norwich, Vermont.

Johnson, M. W. and Moore, J., 1983a, "The Influence of Flow Rate on the Wake in a Centrifugal Impeller," ASME Journal of Engineering for Gas Turbine and Power, Vol. 105, pp. 33~39.

Johnson, M. W. and Moore, J., 1983b, "Secondary Flow Mixing Losses in a Centrifugal Impeller," ASME Journal of Engineering for Gas Turbine and Power, Vol. 105, pp. 24~32.

Jorgenson, P. C. E. and Chima, R. V., 1989, "Explicit Runge-Kutta Method for Unsteady Rotor/Stator Interaction," AIAA Journal, Vol. 27, No. 6, pp. 743~749.

Maksoud, T. M. A. and Johnson, M. W, 1987, "Mean and Turbulent Flow Measurements within the Vaneless Diffuser of a Centrifugal Compressor," Proceedings of the Institution of Mechanical Engineers, International conference publications C263/87.

McDonald, G. B., Lennemann, E. and Howard, J. M. G., 1971, "Measured and Predicted Flow Near the Exit of a Radial-Flow Impeller," ASME Journal of Engineering for Gas Turbine and Power, Vol. 93, No. 4.

Paone, N., Riethmuller, M. L. and Van den Braembussche, R.A., 1989, "Experimental Investigation of the Flow in the Vaneless Diffuser of a Centrifugal Pump by Particle Image Displacement Velocimetry," Experiments in Fluid, Vol.7, pp.371~378.

Westphal, R. V. and Mehta, R. D., 1984, "Crossed Hot-Wire Data Acquisition and Reduction System," NASA TM-85871.